Volume 1 | Number 1 | Jan 2013 | Pages 1–100

# Dalton Transactions

An international journal of inorganic chemistry
www.rsc.org/dalton

ROYAL SOCIETY OF CHEMISTRY

This is an *Accepted Manuscript*, which has been through the Royal Society of Chemistry peer review process and has been accepted for publication.

*Accepted Manuscripts* are published online shortly after acceptance, before technical editing, formatting and proof reading. Using this free service, authors can make their results available to the community, in citable form, before we publish the edited article. We will replace this *Accepted Manuscript* with the edited and formatted *Advance Article* as soon as it is available.

You can find more information about *Accepted Manuscripts* in the **Information for Authors**.

Please note that technical editing may introduce minor changes to the text and/or graphics, which may alter content. The journal's standard **Terms & Conditions** and the **Ethical guidelines** still apply. In no event shall the Royal Society of Chemistry be held responsible for any errors or omissions in this *Accepted Manuscript* or any consequences arising from the use of any information it contains.

www.rsc.org/dalton

**Journal Name**

**Dalton Transactions**

Dynamic Article Links ▶

**ARTICLE TYPE**

# Structural evolvement and thermoelectric properties of Cu$_{3-x}$Sn$_x$Se$_3$ compounds with diamond-like crystal structure

Jing Fan,[a,b,c] Walter Schnelle,[b] Iryna Antonyshyn,[b] Igor Veremchuk,[b] Wilder Carrillo-Cabrera,[b] Xun Shi,[a] Yuri Grin,[b] Lidong Chen*[a]

Polycrystalline samples of Cu$_{3-x}$Sn$_x$Se$_3$ were synthesized in the composition range $x$ = 0.87-1.05. A compositionally induced evolvement from tetragonal via cubic to monoclinic crystal structures is observed, when the composition changes from a Cu-rich to a Sn-rich one. The Cu$_{3-x}$Sn$_x$Se$_3$ materials show
10 a metal-to-semiconductor transition with increasing $x$. Electronic transport properties are governed by charge-carrier concentration which is well described by a linear dispersion-band model. Lattice component of the thermal conductivity is practically independent from x which is attributed to the opposite influence of the atomic ordering and the inhomogeneous distribution of the Cu-Se or Sn-Se bonds with different polarity of in the crystal structure. The highest thermoelectric figure of merit $ZT$ of
15 0.34 is achieved for $x$ = 1.025 at 700 K.

## 1. Introduction

The search for high-efficiency low-cost materials is crucial for advanced thermoelectric (TE) applications such as waste heat recovery and electric power generation. The TE performance of a
20 material is characterized by the dimensionless figure of merit, $ZT$ = $S^2\sigma T/\kappa$, where $S$, $\sigma$, $\kappa$ and $T$ are the Seebeck coefficient, the electrical conductivity, the thermal conductivity, and the absolute temperature, respectively. Cu-based chalcogenide semiconductors with diamond-like structure have attracted a lot of attention lately
25 because of their low thermal conductivity. Good thermoelectric performance has been reported for several compounds, *e.g.*, Cu$_2$ZnSnSe$_4$[1], Cu$_2$SnSe$_3$[2], CuInTe$_2$[3], CuGaTe$_2$[4] and CuFeS$_2$[5].

The crystal structures of these ternary and quaternary chalcogenides are derivatives of either the sphalerite or the
30 wurtzite patterns, which are characterized by a tetrahedral coordination of all atoms. Theoretical calculations on Cu$_2$ZnSnSe$_4$ and Cu$_2$SnS$_3$ suggest that polymorphs with distinct cation distribution may exist with small energy differences between them. Different polymorphs yield similar electronic band
35 structures and DOS, indicating that the cation distribution should have little effect on the electrical transport properties.[6-9] Coexistence of chemically similar and/or structurally different regions within a main phase matrix may be one of the factors contributing to the low thermal conductivity, as was recently
40 shown for the Cu$_2$GeSe$_3$[10] and Cu$_2$SnSe$_3$.[11]

Despite many studies on the thermoelectric properties of Cu$_2$SnSe$_3$,[2, 12-16] previous reports on its crystal structure are contradictory.[17-21] Our recent investigation shows that stoichiometric Cu$_2$SnSe$_3$ crystallizes in a monoclinic structure at
45 low, and in a cubic structure at elevated temperature.[11]

In the present work, by controlling the Cu/Sn ratio, we obtained specimens in the vicinity of the composition Cu$_2$SnSe$_3$ possessing four types of crystal structure with distinct cation ordering. The composition-linked structural relationship is
50 described. Furthermore, the influence of the crystal structure on electrical and thermal properties is discussed.

## 2. Experimental

Polycrystalline samples with nominal composition Cu$_{3-x}$Sn$_x$Se$_3$ ($x$ = 0.87, 0.90, 0.95, 0.975, 1.00, 1.025, 1.05) were synthesized by
55 direct reaction of elemental copper (powder, 99.999%, Chempur), tin (foil, 99.99%, Chempur) and selenium (shot, 99.999%, Alfa Aesar) in evacuated and sealed quartz ampoules. The starting mixtures were heated slowly up to 1173 K and held for 12 h, then cooled down to 850 K in 24 h, followed by annealing at this
60 temperature for 7 days. The obtained ingots were ground into fine powder, cold pressed into pellets, and then annealed at 850 K for additional 7 days to ensure homogeneity of the element distribution. In order to obtain dense bulk samples suitable for thermoelectric properties measurements, spark plasma sintering
65 (SPS) was applied (SPS − 515 ET, Dr. Sinter setup, SDC Fuji Japan). Consolidation was performed by heating to 790 K at 25 K/min under an uniaxial pressure of 60 MPa. This temperature was held for 10 min. The density of the so-produced pellets, determined by the Archimedes method, was >95% of the
70 theoretical value.

Powder X-ray diffraction was carried out on a Huber image plate Guinier camera G670 (Cu$K\alpha_1$ radiation, $\lambda$ = 1.54056 Å, germanium (111) monochromator, 6 × 30 min scans, $3° \leq 2\theta \leq$ 100.3°) at ambient temperature. The lattice parameters were
75 refined using Si ($a$ = 5.4312 Å) as internal standard, with a least-squares refinement method, employing the WinCSD program

package.[22]

The thermal diffusivity $\lambda$ was measured on disk-shaped specimens (diameter 10 mm) using a laser-flash technique employing a Netzsch LFA 427 setup in the temperature range
5 300-700 K in helium atmosphere. The thermal conductivity $\kappa$ was then calculated as $\kappa = C_p d\lambda$, where $d$ is the density and $C_p$ is the Dulong–Petit approximation for the specific heat capacity. For the electrical transport properties measurement, bar-shaped specimens of $1.5 \times 1.5 \times 10$ mm$^3$ were cut with a diamond wire
10 saw from the disk-shaped specimen. Both, electrical resistivity $\rho$ and Seebeck coefficient $S$ were determined simultaneously (ULVAC-RIKO ZEM-3) in the temperature range 300-700 K in helium flow. Hall coefficient $R_H$ and low temperature resistivity $\rho$ were measured employing a dynamic method (TTO, PPMS,
15 Quantum Design) between 2 and 300 K. The charge carrier concentration $p_H$ and carrier mobility $\mu_H$ were calculated according to the equations $p_H \cdot e = R_H^{-1}$ and $\mu_H = (p_H \cdot e \cdot \rho)^{-1}$, respectively, where $e$ is electron charge.

## 3. Results and discussion

20 **3.1 Structural relationship**

With increasing $x$, a structural evolution from tetragonal, via cubic, monoclinic-II to monoclinic-III is observed for the Cu$_{3-x}$Sn$_x$Se$_3$ samples annealed at 850 K. Here, monoclinic-II and III structures refer to the different arrangements of Se-centred
25 tetrahedra in these two modifications, as discussed in Ref. 11. Since these four structures are derivatives of the cubic sphalerite-type, their powder X-ray diffraction patterns exhibit seven main reflections in the range $20° < 2\theta < 95°$. They differ in the splitting of the main reflections (Fig. 1, inset) and/or in the appearance of
30 low-intensity superstructure reflections (Fig. 2). The crystallographic data for the investigated samples are listed in Table 1.
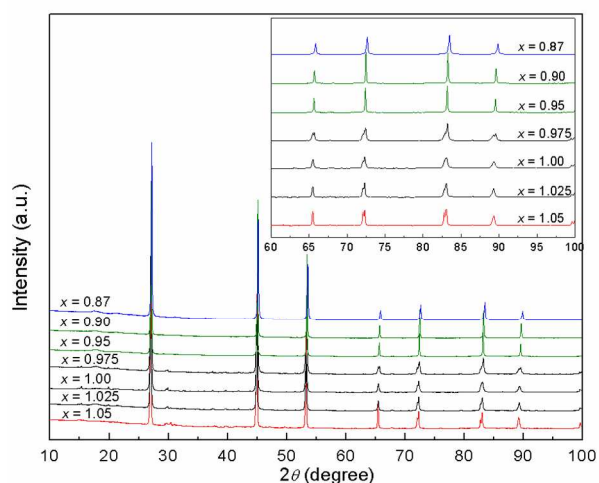


**Fig. 1** Powder X-ray diffraction patterns of Cu$_{3-x}$Sn$_x$Se$_3$ samples. The
35 inset shows an enlargement of the high-angle region.

**Table 1** Crystallographic data of Cu$_{3-x}$Sn$_x$Se$_3$ samples

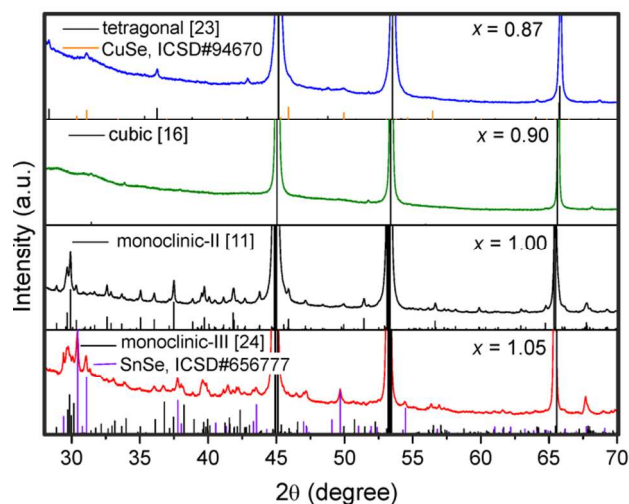| $x$ | Space group | $a$ / Å | $b$ / Å | $c$ / Å | $\beta$ / ° | $V^*$ / Å$^3$ |
|---|---|---|---|---|---|---|
| 0.87 | $I\bar{4}2m$ | 5.6735(3) | | 11.354(1) | | 45.68 |
| 0.90 | $F\bar{4}3m$ | 5.6758(2) | | | | 45.71 |
| 0.95 | $F\bar{4}3m$ | 5.6840(1) | | | | 45.91 |
| 0.975 | $Cc$ | 6.9689(3) | 12.079(1) | 13.391(1) | 99.824(4) | 46.28 |
| 1.00 | $Cc$ | 6.9689(2) | 12.078(1) | 13.3922(4) | 99.833(3) | 46.28 |
| 1.025 | $Cc$ | 6.9721(3) | 12.078(1) | 13.393(1) | 99.86(1) | 46.30 |
| 1.05 | $Cc$ | 6.977(1) | 12.071(1) | 26.493(2) | 94.96(1) | 46.31 |

*per formula unit Cu$_{3-x}$Sn$_x$Se$_3$



**Fig. 2** The superstructure reflections for Cu$_{3-x}$Sn$_x$Se$_3$ samples with
40 different crystal structures. The reflection positions of the main phases are indicated by black bars, the reflection positions of the minority phases CuSe and SnSe are shown by orange and violet bars. The vertical scale is twenty times larger than in Fig. 1.

The superstructure reflections distinguishing each Cu$_{3-x}$Sn$_x$Se$_3$
45 phase are weak in comparison to the main ones; the vertical scale in Fig. 2 is twenty times larger than in Fig. 1. The powder XRD pattern of the sample with $x = 0.87$ was indexed employing the structural model of the tetragonal stannite-type structure[23] (Fig. 3, left), which was originally solved using high-temperature
50 synchrotron diffraction data at 873 K. The position of reflections displayed in Fig. 2 are calculated using the lattice parameters of the $x = 0.87$ sample at room temperature. From the Rietveld refinement, around 4% of the impurity phase CuSe was also observed. For $x = 0.90$ and 0.95, the samples show the cubic
55 structure (Fig. 3, middle left), since only seven intense reflections without splitting were observed in the measured $2\theta$ range (Fig. 2). Around the stoichiometric composition Cu$_2$SnSe$_3$ ($0.975 < x \leq 1.025$), the samples crystallize in the monoclinic-II type[11] (Fig. 3, middle right). In the sample with $x = 0.975$, a slight amount of
60 cubic phase was also observed in addition to the majority monoclinic-II phase. Because the cubic phase has smaller unit cell dimensions than the monoclinic-II phase, its presence was discerned by peaks flanking the intense reflections of the monoclinic-II structure at higher diffraction angles (Figs. 1, 2).
65 The sample with $x = 1.05$ crystallizes in the monoclinic-III structure[24] (Fig. 3, right) along with about 5% of impurity phase SnSe. For $x \geq 1.025$, the amount of SnSe increases with the tin content. During the preparation, SnSe forms from the melt above 1000 K; the annealing at 850 K was probably not sufficient to
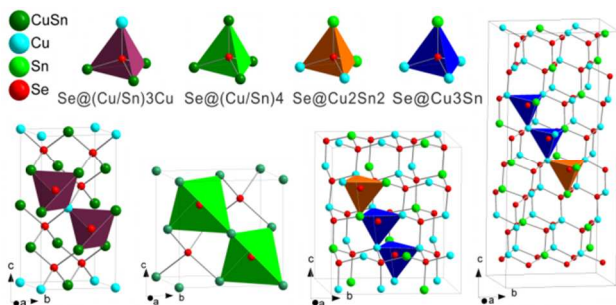
**Fig. 3** Crystal structures of $Cu_{3-x}Sn_xSe_3$ phases: (upper row) the selenium environment; (bottom row, from left to right) projections of the tetragonal, cubic, monoclinic-II, and monoclinic-III structures.

5 completely remove this phase from the reaction products.

The four observed crystal structures show distinct cation distributions within the basic sphalerite-like matrix (Fig. 3). Tetrahedral structural units $Se@(Cu/Sn)_4$ in the lattice have different levels of distortion, indicated by various ranges of 10 interatomic distances and angles in these structures (Table 2). This compositionally-induced structural evolution of $Cu_{3-x}Sn_xSe_3$ may arise from different atomic radii ($r_{Cu}$ = 1.28 Å, $r_{Sn}$ = 1.58 Å [25]) and electronic configurations of the Cu and the Sn atoms. A high concentration of larger Sn atoms ($x$ = 1.05) leads to the 15 appearance of the monoclinic-III structure with a large variety of interatomic distances and angles (Table 2). The arrangement of tetrahedral units $Se@Cu_3Sn$ and $Se@Cu_2Sn_2$ in the monoclinic-III structure differs from that in the monoclinic-II one which exists around the composition $Cu_2SnSe_3$. Both have distorted 20 tetrahedral building units $Se@Cu_3Sn$ and $Se@Cu_2Sn_2$ with bond distances and angles varying slightly less than in the monoclinic-III phase. Increasing the amount of smaller Cu atoms leads locally to a larger amount of the $Se@Cu_3Sn$ (or even appearance of the $Se@Cu_{4-x}Sn_x$ with x < 1) units, allowing – in average – 25 'perfect' $Se@(Cu/Sn)_4$ tetrahedra in the cubic sphalerite-type structure. Further increase in Cu content again gives rise to the ordering of the $Se@Cu_3Sn$ and $Se@Cu_{4-x}Sn_x$ units and to the doubling of the unit cell along the [001] direction.

Due to the atomic radii difference between Cu and Sn, $Cu_{3-x}Sn_xSe_3$ samples exhibit an increase in the unit cell volume per 30 formula unit with increasing Sn content (Table 1). The increase of the unit cell volume for the non-ordered cubic and partially ordered tetragonal phases is stronger than that of the ordered monoclinic phases, *i.e.* the pure size effect on cell volume is partially compensated by ordering of Cu and Sn in the structure. 35

**Table 2** The interatomic distances and angles in the $Cu_{3-x}Sn_xSe_3$ structures

| Crystal structure; x | Distances (/ Å) | | Angles M - Se - M (/ °) |
|---|---|---|---|
| | Cu - Se | Sn - Se | |
| Tetragonal[23] | 2.457(1) - 2.470(1) | 2.549(1) | 107.86(4)- 110.87(4) |
| Cubic[19] | 2.463 | | 109.47 |
| Monoclinic-II[11] | 2.356(6) - 2.491(6) | 2.484(5) - 2.580(5) | 102.86(2) - 115.22(2) |
| Monoclinic-III[24] | 2.380(5) - 2.495(5) | 2.488(3) - 2.627(3) | 104.8(2) - 115.9(2) |
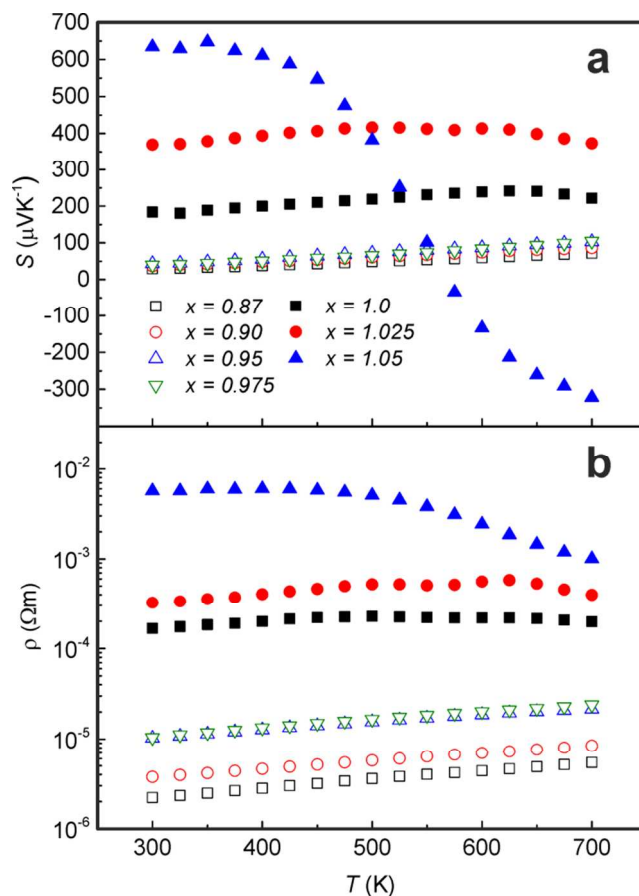


40 **Fig. 4** Temperature dependence of Seebeck coefficient $S$ (top) and electrical resistivity $\rho$ (bottom) for $Cu_{3-x}Sn_xSe_3$ samples.

### 3.2 Electronic transport properties

Due to the different contributions to the charge carrier concentration, the variation in Cu/Sn ratio has a huge influence 45 on the electrical properties, allowing the Seebeck coefficient to range from 21 to 634 $\mu VK^{-1}$ and the electrical resistivity from $10^{-6}$ to $10^{-3}$ $\Omega m$ (Fig. 4). With increasing $x$, the temperature dependence of the Seebeck coefficient and the electrical resistivity exhibits a transition from degenerate to intrinsic 50 semiconducting behaviour. Except for $x$ = 1.05, the samples show positive Seebeck coefficients in the whole temperature range, indicating p-type conduction, which is confirmed further (see below) by the positive Hall coefficient. The electrical resistivity and the Seebeck coefficients of all Cu-rich samples ($x \leq 0.975$) 55 increase approximately linearly with rising temperature, a typical behaviour of a heavily doped semiconductor. These samples may be formulated as $Cu_{2+y}Sn_{1-y}Se_3$ ($y$ = 1 - $x$), *i.e.*, as self-doped like quaternary Cu-based chalcogenides $Cu_{2+x}Zn_{1-x}SnSe_4$,[26] $Cu_{2+x}Cd_{1-x}SnSe_4$[27] or $Cu_{2+x}Zn_{1-x}GeSe_4$.[28] According to simple charge 60 counting, each Cu substituting Sn should yield three holes. The room-temperature charge carrier concentrations calculated this way agree quite well with the experimental values (Fig. 5, solid line). The electrical resistivity and the Seebeck coefficient of $Cu_2SnSe_3$ and Sn-rich samples ($x \geq 1.00$) increase first and then 65 decrease with rising temperature. This is most probably caused by excitation of minority charge carriers across the band gap. As $x$

increases further, the onset of intrinsic excitations moves to lower temperature. The sign change of the Seebeck coefficient above 550 K was observed in $Cu_{1.95}Sn_{1.05}Se_3$ sample with monoclinic-III structure. One may suggest that this Sn-rich composition,
5 generating large amounts of $Sn_{Cu}$ (*i.e.*, tin on the copper position), compensates the holes and results in low carrier concentrations. At elevated temperature, the thermal excitation allows to move the Fermi level towards the band edge, and then further to the anti-bonding states.
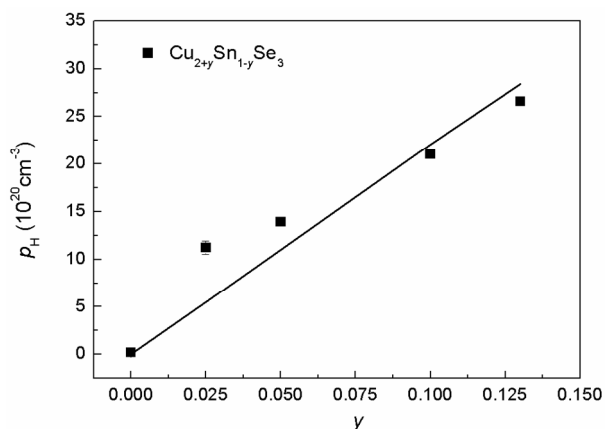


10
**Fig. 5** Room-temperature charge-carrier concentration $p_H$ *vs*. self-doping concentration for $Cu_{2+y}Sn_{1-y}Se_3$. The solid line indicates the expected charge-carrier concentration according to formal charge counting (cf. text).

15 The low-temperature electronic transport properties of $Cu_{3-x}Sn_xSe_3$ samples are shown in Fig. 6. The electrical resistivity of Cu-rich samples increases almost linearly with temperature (Fig. 6a), consistent with high-temperature data. All Cu-rich samples exhibit quite large carrier concentrations of the order $10^{21}$ cm$^{-3}$,
20 which remain essentially constant across the temperature range, being in line with their origin from heavy doping (Fig. 6b). Their mobility deviates from a $T^{-3/2}$ dependence, indicating a mixture of charge-carrier scattering mechanisms, such as acoustic phonons, carrier–carrier and ionized impurity. This mixture is in agreement
25 with the substitutional and compositional disorder in the crystal structure. The carrier concentration of Sn-rich samples is several orders of magnitude smaller than that of Cu-rich samples. The charge-carrier mobility of Sn-rich samples follows the $T^{-3/2}$ dependence around room temperature, which suggests the
30 dominance of acoustic phonon scattering. Around 50-150 K the Sn-rich samples display a minimum for both carrier concentration and electrical resistivity and a peak for mobility is observed in this temperature region (Fig. 6c). Thermally activated hopping transport in an impurity band might be mainly responsible for the
35 increase in mobility; above 140 K both impurity and valence bands contribute.[29] Considering Cu vacancies as a common defect in diamond-like compounds like CuInSe$_2$,[30] the impurity is most likely $V_{Cu}$ rather than selenium interstitials Se$_i$ as proposed in Ref. 31.
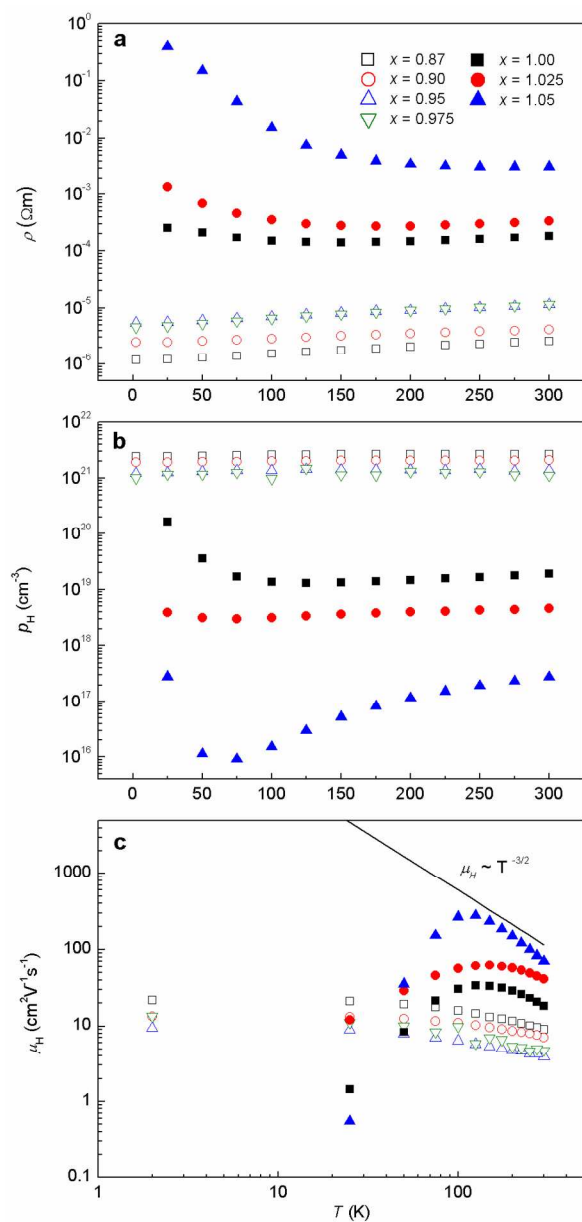


40
**Fig. 6** Temperature dependence of electrical resistivity $\rho$ (top), carrier concentration $p_H$ (middle) and Hall mobility $\mu_H$ (bottom) for $Cu_{3-x}Sn_xSe_3$ samples. The solid line represents the $\mu_H \sim T^{-3/2}$ relationship.
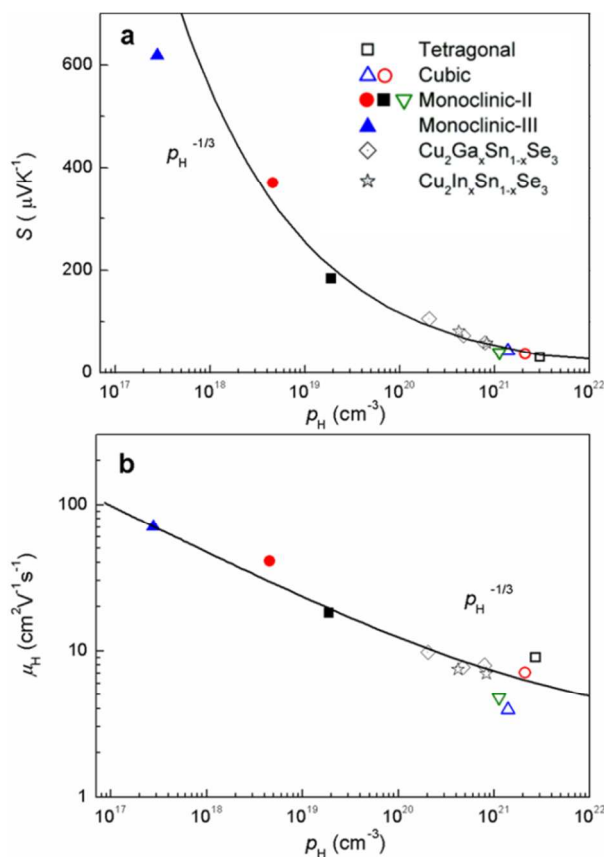
**Fig. 7** Seebeck coefficient $S$ and Hall mobility $\mu_H$ of $Cu_{3-x}Sn_xSe_3$, $Cu_2Ga_xSn_{1-x}Se_3$ (Ref. 16) and $Cu_2In_xSn_{1-x}Se_3$ (Ref. 2) as a function of charge carrier concentration $p_H$ at 300 K. The solid lines represent the $S \sim$
5 $p_H^{-1/3}$ and $\mu_H \sim p_H^{-1/3}$ relationships.

Theoretical calculations predict that the cation distribution in the different polymorphs has a small influence on the electrical properties of Cu-based diamond-like compounds at the given compostition.[5-8] The present experimental work reveals the
10 connection between the structural evolution in the compounds $Cu_{3-x}Sn_xSe_3$ caused mainly by a variation in the charge-carrier concentration and their electronic transport properties (Fig. 7). The data for $Cu_2Ga_xSn_{1-x}Se_3$[16] and $Cu_2In_xSn_{1-x}Se_3$[2] are included for comparison. A good fit was obtained for both, Seebeck
15 coefficient and Hall mobility, of all samples but one (with $x =$ 1.05) using the linear band-dispersion model after Ioffe[32, 33], which was previously applied for intermetallic filled skutterudites and clathrates.[34-36] The experimental data follow roughly the same $S \sim p_H^{-1/3}$ and $\mu_H \sim p_H^{-1/3}$ dependence, indicating that the
20 electronic transport properties of $Cu_{3-x}Sn_xSe_3$ are clearly governed by the carrier concentration. As already discussed in Ref. 16, Ga and In substitution on the Sn site barely influences the band structure, so the Seebeck coefficient and mobility of $Cu_2Ga_xSn_{1-x}Se_3$[16] and $Cu_2In_xSn_{1-x}Se_3$[2] follow the same trend as in the $Cu_{3-x}Sn_xSe_3$ system. However, Sn-by-Cu substitution leads to a large
25 variation in carrier amount; in contrast, trivalent dopants Ga and In allow a fine tuning of charge carrier concentration between $10^{20} \sim 10^{21}$ cm$^{-3}$.

### 3.3 Thermal transport behaviour



30
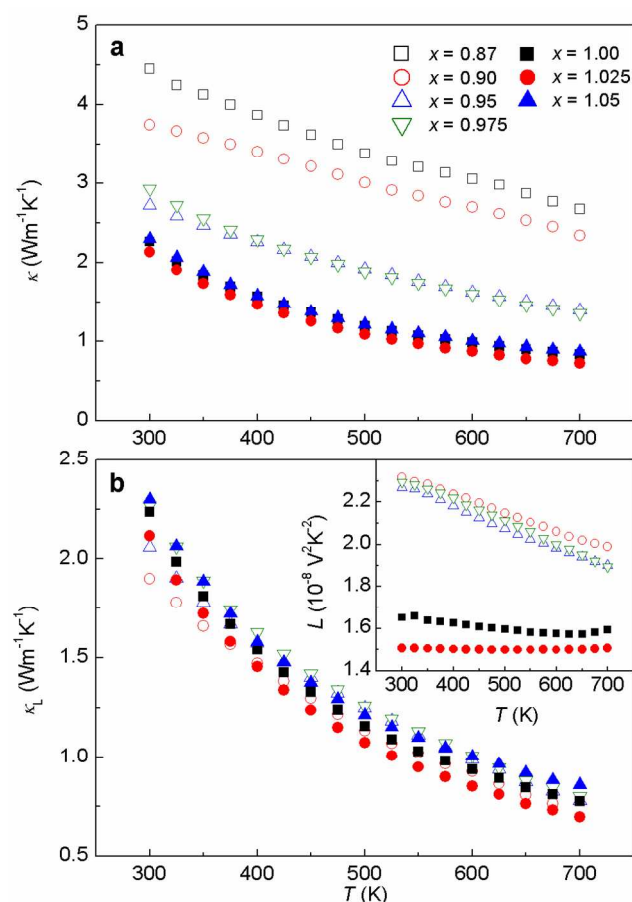
**Fig. 8** Temperature dependence of the total thermal conductivity $\kappa$ and the lattice thermal conductivity $\kappa_L$ for $Cu_{3-x}Sn_xSe_3$ samples. The inset in (b) shows the calculated temperature-dependent Lorenz number $L$.

The temperature dependence of the total thermal conductivity
35 is shown in Fig. 8a. To obtain the lattice thermal conductivity $\kappa_L$, the electronic component $\kappa_e$ of thermal conductivity was subtracted from the total thermal conductivity using the Wiedemann-Franz law ($\kappa_e = LT/\rho$; $\kappa = \kappa_L + \kappa_e$). Temperature-dependent Lorenz numbers $L$ were calculated within the single
40 parabolic-band approximation using eqs. 1-3 (Ref. 37).

$$L = \frac{k_B^2}{e^2} \frac{(1+\lambda)(3+\lambda)F_\lambda(\eta)F_{\lambda+2}(\eta)-(2+\lambda)^2 F_{\lambda+1}^2(\eta)}{(1+\lambda)^2 F_\lambda^2(\eta)} \quad (1)$$

$$F_j(\eta) = \int_0^\infty \frac{\xi^j d\xi}{1+\exp(\xi-\eta)} \quad (2)$$

$$S = \frac{k_B}{e}\left(\frac{(2+\lambda)F_{1+\lambda}(\eta)}{(1+\lambda)F_\lambda(\eta)} - \eta\right) \quad (3)$$

$k_B$ is the Boltzmann constant, $F_j(\eta)$ are the Fermi integrals, and $\xi$
45 is the reduced carrier energy. The reduced chemical potential $\eta$ is determined from the experimental Seebeck coefficient of each sample at various temperatures. The parameter $\lambda$ gives the exponent of the energy dependence of the charge carrier mean free path. Here, the acoustic phonon scattering ($\lambda = 0$) is taken as
50 the dominant scattering mechanism. Even though around room temperature, the Cu-rich samples exhibit mixed carrier scattering, the assumption that acoustic phonon scattering dominates at high temperature is still reasonable. The calculated Lorenz numbers are smaller than the metallic limit of $2.45 \times 10^{-8}$ V$^2$K$^{-2}$, decreasing

from 2.32 to $1.50 \times 10^{-8}$ $V^2K^{-2}$ at 300 K when the composition changes from Cu-rich to Sn-rich (the inset in Fig. 8b). Since the sample with $x = 1.05$ exhibits a change in the sign of the Seebeck coefficient, and the single parabolic band model is not valid at high temperature, the Lorenz number of $1.49 \times 10^{-8} V^2 K^{-2}$ obtained up to 475 K was used for the estimation above this temperature. The sample with $x = 0.87$ has very low electrical resistivity so that the resulting electronic thermal conductivity is very large in comparison to the total one. This does not allow for a reliable estimation of the lattice part of the thermal conductivity at high temperature. Thus, the sample is not displayed in Fig. 8b.

The estimated lattice thermal conductivities of $Cu_{3-x}Sn_xSe_3$ compounds are quite close, all below 2.35 $Wm^{-1}K^{-1}$, being much less than that of diamond with the prototype structure. This may be correlated with different atomic interactions. All bonds in diamond are non-polar and equal, whereas the structures of $Cu_{3-x}Sn_xSe_3$ compounds are characterized by inhomogeneous Cu-Se and Sn-Se bonding with different polarity, as proposed for monoclinic-II $Cu_2SnSe_3$.[11] Moreover, Cu and Sn are completely or partially disordered in the cubic and the tetragonal structure, while being ordered in the two monoclinic structures. Both inhomogeneous bonding and atomic disordering can be regarded as structural defects,[38] increasing scattering of heat-carrying phonons and reducing the lattice thermal conductivity. Thus, the inhomogeneity of the bonding and the atomic ordering are influencing the lattice thermal conductivity in opposite ways. The sum of these two factors together with the small volume effects by Cu/Sn substitution (cf. Table 1) may thus be responsible for the similar lattice thermal conductivity of all $Cu_{3-x}Sn_xSe_3$ compounds studied here.

### 3.4 Figure of merit



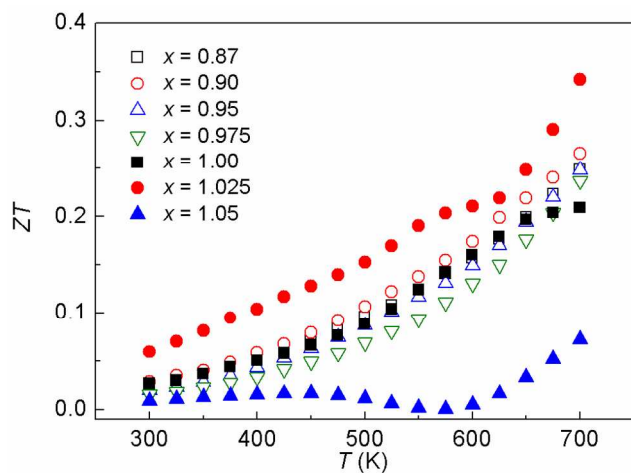**Fig. 9** Temperature dependence of figure of merit $ZT$ for $Cu_{3-x}Sn_xSe_3$ samples.

As a combination of both thermal and electronic transport properties, the figure of merit $ZT$ for $Cu_{3-x}Sn_xSe_3$ samples does not exhibit a clear relationship with the Cu/Sn ratio (Fig. 9). The sample with $x = 1.025$ shows a maximum $ZT$ of 0.34 at 700 K, being only slightly lower than the best results reported in Ga- and In-doped $Cu_2SnSe_3$.[2, 16] Compared to the large variation in carrier number per one substitution atom in $Cu_{3-x}Sn_xSe_3$, Ga and In contribute less valence electrons than Sn and allow for a more

precise control of the carrier concentration. It is worth noticing that a change of the Cu/Sn ratio can influence both structure and properties of $Cu_2SnSe_3$-based materials When assessing the role of extrinsic doping on the properties, special care should be taken to minimize the uncertainty caused by deviations in composition.

## 4. Conclusions

The compounds $Cu_{3-x}Sn_xSe_3$ with four different crystal structures have been synthesized. The Sn-by-Cu substitution influences both the crystal structure and properties of the compounds. When the composition changes from Cu-rich to Sn-rich, the samples exhibit a transition from tetragonal via cubic to monoclinic structures. The difference in electronic configuration and atomic sizes of Cu and Sn atoms are responsible for this structural evolvement. The atomic size is controlling the degree of distortion in the Se-centred tetrahedral building units in the crystal structures. The concomitant evolvement from degenerate to intrinsic p-type semiconducting behaviour observed in electronic transport properties is mainly caused by the differences in electronic configuration and subsequent charge carrier concentration. The Seebeck coefficient and mobility of $Cu_{3-x}Sn_xSe_3$ compounds were well fitted using the linear dispersion-band model. The electronic part of the phonon transport of $Cu_{3-x}Sn_xSe_3$ compounds is also dependent on the charge carrier concentration. In contrast, the lattice component of the thermal conductivity is practically independent from x which is attributed to the opposite influence of the atomic ordering and the inhomogeneous distribution of the Cu-Se or Sn-Se bonds with different polarity of in the crystal structure. The maximum $ZT$ value of 0.34 is achieved for the sample with $x = 1.025$ at 700 K.

### Acknowledgements

### Notes

*[a] State Key Laboratory of High Performance Ceramics and Superfine Microstructure, Shanghai Institute of Ceramics, Chinese Academy of Sciences, 1295 Dingxi Road, 200050 Shanghai, China. E-mail: cld@mail.sic.ac.cn.*
*[b] Max-Planck-Institut für Chemische Physik fester Stoffe, Nöthnitzer Str. 40, 01187 Dresden, Germany.*
*[c] University of Chinese Academy of Sciences, 19 Yuquan Road, 100049 Beijing, P.R. China.*

### References

1.   X. Y. Shi, F. Q. Huang, M. L. Liu and L. D. Chen, *Appl. Phys. Lett.*, 2009, 94, 122103.
2.   X. Y. Shi, L. L. Xi, J. Fan, W. Q. Zhang and L. D. Chen, *Chem. Mat.*, 2010, 22, 6029-6031.
3.   R. H. Liu, L. L. Xi, H. L. Liu, X. Shi, W. Q. Zhang and L. D. Chen, *Chem. Commun.*, 2012, 48, 3818-3820.
4.   T. Plirdpring, K. Kurosaki, A. Kosuga, T. Day, S. Firdosy, V. Ravi, G. J. Snyder, A. Harnwunggmoung, T. Sugahara, Y.

Ohishi, H. Muta and S. Yamanaka, *Adv. Mater.*, 2012, 24, 3622-3626.

5. N. Tsujii and T. Mori, *Appl. Phys. Express*, 2013, 6, 043001.
6. C. Sevik and T. Cagin, *Appl. Phys. Lett.*, 2009, 95, 112105.
7. C. Sevik and T. Cagin, *Phys. Rev. B*, 2010, 82, 045202.
8. S. Y. Chen, A. Walsh, Y. Luo, J. H. Yang, X. G. Gong and S. H. Wei, *Phys. Rev. B*, 2010, 82, 195203.
9. Y. T. Zhai, S. Y. Chen, J. H. Yang, H. J. Xiang, X. G. Gong, A. Walsh, J. Kang and S. H. Wei, *Phys. Rev. B*, 2011, 84, 075213.
10. M. Ibanez, R. Zamani, W. H. Li, D. Cadavid, S. Gorsse, N. A. Katcho, A. Shavel, A. M. Lopez, J. R. Morante, J. Arbiol and A. Cabot, *Chem. Mat.*, 2012, 24, 4615-4622.
11. J. Fan, W. Carrillo-Cabrera, L. Akselrud, I. Antonyshyn, L. Chen and Y. Grin, *Inorg. Chem.*, 2013, 52, 11067-11074.
12. E. J. Skoug, J. D. Cain and D. T. Morelli, *J. Alloy. Compd.*, 2010, 506, 18-21.
13. E. J. Skoug, J. D. Cain and D. T. Morelli, *J. Electron. Mater.*, 2012, 41, 1232-1236.
14. X. Lu and D. T. Morelli, *J. Electron. Mater.*, 2012, 41, 1554-1558.
15. M. Ibanez, D. Cadavid, U. Anselmi-Tamburini, R. Zamani, S. Gorsse, W. H. Li, A. M. Lopez, J. R. Morante, J. Arbiol and A. Cabot, *J. Mater. Chem. A*, 2013, 1, 1421-1426.
16. J. Fan, H. L. Liu, X. Y. Shi, S. Q. Bai, X. Shi and L. D. Chen, *Acta Mater.*, 2013, 61, 4297-4304.
17. L. S. Palatnik, V. M. Koshkin, L. P. Galchinetskii, V. I. Kolesnikov and Y. F. Komnik, *Sov. Phys., Solid State*, 1962, 4, 1052-1053.
18. J. Rivet, P. Laruelle and J. Flahaut, *Comptes Rendus Hebdomadaires des Seances de L' Academie des Sciences*, 1963, 257, 161-&.
19. B. B. Sharma, R. Ayyar and H. Singh, *Phys. Status Solidi A*, 1977, 40, 691-696.
20. H. Hahn, W. Klingen, P. Ness and H. Schulze, *Naturwissenschaften*, 1966, 53, 18-&.
21. J. Rivet, *Annales De Chimie France*, 1965, 10, 243-&.
22. L. Akselrud and Y. Grin, *J. Appl. Crystallogr.*, 2014, 47, 803-805.
23. J. Fan, W. Carrillo-Cabrera, I. Antonyshyn, Y. Prots, I. Veremchuk, W. Schnelle, C. Drathen, L. D. Chen and Y. Grin, 2014, accepted by *Chem. Mat.*.
24. L. D. Gulay, M. Daszkiewicz, T. A. Ostapyuk, O. S. Klymovych and O. F. Zmiy, *Acta Crystallogr. Sect. C-Cryst. Struct. Commun.*, 2010, 66, I58-I60.
25. J. Emsley, *The Elements*, Clarendon Press, Oxford, 1998.
26. M. L. Liu, F. Q. Huang, L. D. Chen and I. W. Chen, *Appl. Phys. Lett.*, 2009, 94, 202103.
27. M. L. Liu, I. W. Chen, F. Q. Huang and L. D. Chen, *Adv. Mater.*, 2009, 21, 3808-3812.
28. W. G. Zeier, A. LaLonde, Z. M. Gibbs, C. P. Heinrich, M. Panthofer, G. J. Snyder and W. Tremel, *J. Am. Chem. Soc.*, 2012, 134, 7147-7154.
29. J. Y. Cho, X. Shi, J. R. Salvador, J. Yang and H. Wang, *J. Appl. Phys.*, 2010, 108, 073713.
30. S. B. Zhang, S. H. Wei, A. Zunger and H. Katayama-Yoshida, *Phys. Rev. B*, 1998, 57, 9642-9656.
31. G. Marcano, C. Rincon, L. M. de Chalbaud, D. B. Bracho and G. S. Perez, *J. Appl. Phys.*, 2001, 90, 1847-1853.
32. A. F. Ioffe, *Semiconductors in the Modern Physics*, Publishing House of the Academy of Sciences USSR, Moscow, 1954.
33. A. F. Ioffe, *Semiconductor Thermoelements and Thermoelectric Cooling*, Infosearch Limited, 1957.
34. T. Caillat, A. Borshchevsky and J. P. Fleurial, *J. Appl. Phys.*, 1996, 80, 4442-4449.
35. D. J. Singh and W. E. Pickett, *Phys. Rev. B*, 1994, 50, 11235-11238.
36. X. Shi, J. Yang, S. Q. Bai, J. H. Yang, H. Wang, M. F. Chi, J. R. Salvador, W. Q. Zhang, L. D. Chen and W. Wong-Ng, *Adv. Funct. Mater.*, 2010, 20, 755-763.
37. A. F. May, E. S. Toberer, A. Saramat and G. J. Snyder, *Phys. Rev. B*, 2009, 80, 125205.
38. L. T. K. Nguyen, U. Aydemir, M. Baitinger, E. Bauer, H. Borrmann, U. Burkhardt, J. Custers, A. Haghighirad, R. Hofler, K. D. Luther, F. Ritter, W. Assmus, Y. Grin and S. Paschen, *Dalton Trans.*, 2010, 39, 1071-1077.

Table of Contents
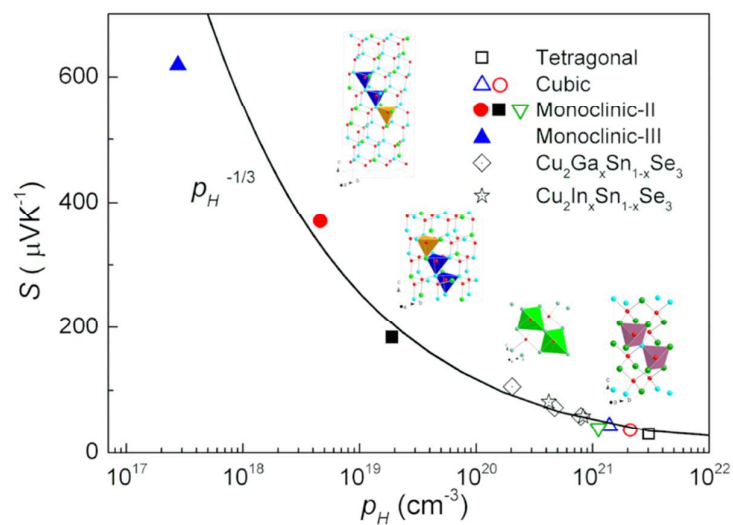


When the composition changes from a Cu-rich to a Sn-rich one, $Cu_{3-x}Sn_xSe_3$ shows a metal-to-semiconductor transition with increasing $x$.